

UCLA

UCLA Previously Published Works

Title

Off-resonance insensitive complementary SPAtial Modulation of Magnetization (ORI-CSPAMM) for quantification of left ventricular twist

Permalink

<https://escholarship.org/uc/item/02q885z5>

Journal

Journal of Magnetic Resonance Imaging, 39(2)

ISSN

1053-1807

Authors

Reyhan, Meral
Natsuaki, Yutaka
Ennis, Daniel B

Publication Date

2014-02-01

DOI

10.1002/jmri.24154

Peer reviewed

Off-Resonance Insensitive Complementary SPATial Modulation of Magnetization (ORI-CSPAMM) for Quantification of Left Ventricular Twist

Meral Reyhan, PhD,^{1,2*} Yutaka Natsuaki, PhD,³ and Daniel B. Ennis, PhD^{1,2}

Purpose: To evaluate Off Resonance Insensitive Complementary SPATial Modulation of Magnetization (ORI-CSPAMM) and Fourier Analysis of STimulated echoes (FAST) for the quantification of left ventricular (LV) systolic and diastolic function and compare it with the previously validated FAST+SPAMM technique.

Materials and Methods: LV short-axis tagged images were acquired with ORI-CSPAMM and SPAMM in healthy volunteers ($n=13$). The FAST method was used to automatically estimate LV systolic and diastolic twist parameters from rotation of the stimulated echo and stimulated anti-echo about the middle of k -space subsequent to ~ 3 min of user interaction.

Results: There was no significant difference between measures obtained for FAST+ORI-CSPAMM and FAST+SPAMM for mean peak twist ($12.9 \pm 3.4^\circ$ versus $11.9 \pm 4.0^\circ$; $P=0.4$), torsion ($3.3 \pm 0.9^\circ/\text{cm}$ versus $2.9 \pm 1.0^\circ/\text{cm}$, $P=0.3$), circumferential-longitudinal shear angle ($9.1 \pm 3.0^\circ$ versus $8.2 \pm 3.4^\circ$, $P=0.3$), twisting rate ($79.6 \pm 20.2^\circ/\text{s}$ versus $68.2 \pm 23.4^\circ/\text{s}$, $P=0.1$), untwisting rate ($-117.5 \pm 31.4^\circ/\text{s}$ versus $-106.6 \pm 32.4^\circ/\text{s}$, $P=0.3$), normalized untwisting rate ($-9.3 \pm 2.0/\text{s}$ versus $-9.9 \pm 4.4/\text{s}$, $P=0.7$), and time of peak twist (281 ± 18 ms versus 293 ± 25 ms, $P=0.04$). FAST+ORI-CSPAMM also provided measures of duration of untwisting (148 ± 21 ms) and the ratio of rapid untwisting to peak twist (0.9 ± 0.3). Bland-Altman analysis of FAST+ORI-CSPAMM and FAST+SPAMM twist data demonstrates excellent agreement with a bias of -0.1° and 95% confidence intervals of (-1.0° , 3.2°).

Conclusion: FAST+ORI-CSPAMM is a semi-automated method that provides a quick and quantitative assessment of LV systolic and diastolic twist and torsion. ORI-CSPAMM corrects off-resonance accrued during tagging

preparation and readout and visibly removes chemical shift from the tagging pattern, which confers greater robustness to the derived quantitative measures.

Key Words: tagging; twist; off-resonance; diastole; left ventricle

J. Magn. Reson. Imaging 2014;39:339–345.

© 2013 Wiley Periodicals, Inc.

IN GENERAL, OFF-resonance due to field inhomogeneity, susceptibility, and chemical shift leads to unwanted signal characteristics. In quantitative motion encoding sequences and measurements derived from them such as SPATial Modulation of Magnetization (SPAMM) tagging (1), DENSE (2), HARP (3), Fourier Analysis of STimulated echoes (FAST) (4), and phase contrast (5), off-resonance can lead to perturbations of the tagging pattern or inaccuracies in the signal phase estimates. Left ventricular (LV) twist can be measured from rotating tagging patterns, but can suffer inaccuracies as a consequence of off-resonance derived perturbations of the tagging pattern. Minimizing the effects of off-resonance is important to eliminating systematic and quantitative measurement errors.

Fahmy et al (6) used the off-resonance of fat and a uniquely modified Complimentary SPATial Modulation of Magnetization (CSPAMM) encoding method to cancel the fat signal in each cardiac phase. The modifications to the CSPAMM sequence included: (i) an inversion of the tagging gradient used during the second SPAMM measurement, which reverses the position of the stimulated echo and stimulated anti-echo in k -space; and (ii) prolonging the tag encoding duration so that the phase of chemically shifted fat is 90° relative to on-resonance water, which results in cancellation of the fat signal after image subtraction. The combination of these modifications leads to suppression of the fat signal in each CPSAMM tagged image. The second modification, however, only works precisely for a single isochromat (3.5 ppm shift in their case). In addition, at higher field strengths, the duration of the motion encoding gradient needed to cancel the fat signal may be too short to allow the tagging gradient to be played, especially for closely spaced tags.

¹Department of Radiological Sciences, David Geffen School of Medicine, University of California, Los Angeles, California, USA

²Biomedical Physics Interdepartmental Program, University of California, Los Angeles, California, USA

³Siemens Healthcare Los Angeles, California, USA

Contract grant sponsor: NIH/NHLIB; Contract grant number: HL087614.

*Address reprint requests to: M.R., Department of Radiological Sciences, Division of Cardiovascular Imaging, Peter V. Ueberroth Building, Suite 1417, 10945 LeConte Avenue, Los Angeles, CA 90095-7206. E-mail: meral@ucla.edu

Received October 3, 2012; Accepted March 5, 2013

DOI 10.1002/jmri.24154

View this article online at wileyonlinelibrary.com.

Herein, we propose an alternative modification to the CSPAMM sequence that compensates for all forms of off-resonance and requires no a priori knowledge of the chemically shifted isochromat to be corrected. Hence, the proposed solution is independent of the frequency spectrum of off-resonant moieties and of main-field strength.

The improved tagging contrast generated by CSPAMM (7) compared with SPAMM is the result of radiofrequency (RF) phase cycling the second tagging pulse by 180° and subtracting the phase cycled images from each other, which effectively cancels the relaxed component of the magnetization from the tagging information. Off-resonance phase accumulation occurs during both motion encoding (tagging gradients and RF pulses) and during imaging. Off-Resonant Insensitive-CSPAMM (ORI-CSPAMM) is a tagging pulse sequence that corrects off-resonance accrued during tagging preparation and readout and visibly removes chemical shift from the tagging pattern.

In this study, we seek to evaluate ORI-CSPAMM and Fourier Analysis of STimulated echoes (FAST), an image analysis technique that measures LV rotation from tagged MR images, for the quantification of LV systolic and diastolic function and compare it with the previously validated FAST+SPAMM technique. To evaluate the quantitative ability of FAST+ORI-CSPAMM, a comparison between a known and validated standard (FAST+SPAMM in normal subjects) is demonstrated.

THEORY

Off-Resonance During Motion Encoding

Figure 1A shows the pulse sequence timing diagram for the two conventional 1-1 SPAMM experiments used to generate CSPAMM (7) tagging contrast. If the initially available longitudinal magnetization is denoted by M_z^0 , then the state of the magnetization immediately after the first 90° RF-pulse is:

$$\vec{M} = \begin{bmatrix} M_z^0 \sin(\theta) \\ M_z^0 \cos(\theta) \\ 0 \end{bmatrix} = \begin{bmatrix} 0 \\ M_z^0 \\ 0 \end{bmatrix} \quad [1]$$

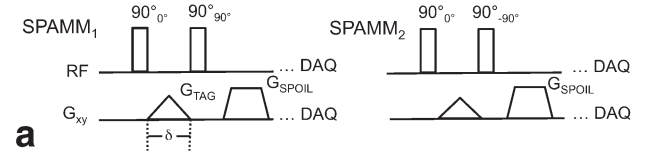
Where, θ in general, denotes the phase of the RF pulse (0° RF phase indicates rotation about the $+x$ -axis and 90° is phased about the $+y$ -axis) and $\theta = 0^\circ$, in particular.

In general, the phase ξ accumulated by an isochromat in the rotating coordinate frame at position \vec{r} in the presence of both a magnetic field gradient \vec{G} and an off-resonant field B_{Off} is:

$$\xi(\vec{r}) = \gamma \left(\int_0^\delta (\vec{G}(t) \cdot \vec{r} + B_{Off}(\vec{r})) dt \right) \quad [2]$$

Where γ is the gyromagnetic ratio for hydrogen nuclei and δ is the duration of the gradient. If the spins are stationary during the time of integration δ and the off-resonance field is stable in time, then:

CSPAMM



ORI-CSPAMM

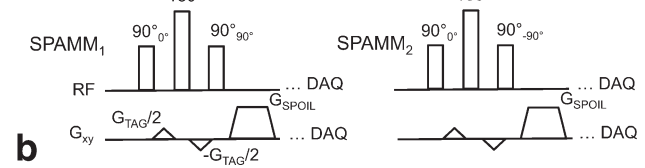


Figure 1. The conventional CSPAMM pulse sequence diagram (a) illustrates the phase-cycling used to create the complementary tagging pattern. The Off-Resonant Insensitive CSPAMM (ORI-CSPAMM) pulse sequence diagram (b) depicts the two phase-cycling loops (SPAMM₁ and SPAMM₂) and the tagging gradient, which has been divided and the 180° refocusing RF pulse, which has been added to correct for off-resonance effects that accrue during motion encoding.

$$\xi(\vec{r}) = \gamma (\vec{M}_0 \cdot \vec{r} + B_{Off}(\vec{r}) \cdot \delta) \quad [3]$$

This equation indicates that the phase of the isochromats will be spatially dependent (first term of Eq. [(3)]) with a spatial shift (second term of Eq. [(3)]) that depends on the magnitude of the off-resonance field at position \vec{r} . Therefore, the magnetization after the motion encoding gradient can be described as:

$$\vec{M} = \begin{bmatrix} -M_z^0 \sin(\xi(\vec{r})) \\ M_z^0 \cos(\xi(\vec{r})) \\ 0 \end{bmatrix} \quad [4]$$

Consequently, in the presence of off-resonance the tagging pattern induced by the applied gradient will be spatially shifted within off-resonant tissues such as fat relative to on-resonance water. Herein, we ignore wavelength changes as a consequence of the chemical shift frequency offset.

The off-resonance effects during motion encoding can be refocused by splitting the motion encoding gradient in half, inserting a hard refocusing pulse, and inverting the second-half of the motion encoding gradient (Fig. 1B). The accumulated signal phase immediately before the refocusing pulse is:

$$\xi_1(\vec{r}) = \gamma \left(\frac{\vec{M}_0}{2} \cdot \vec{r} + B_{Off}(\vec{r}) \cdot \delta \right) \quad [5]$$

After the application of the refocusing pulse the sign of Eq. [(5)] changes. The phase accumulated during the interval after the refocusing pulse is:

$$\xi_2(\vec{r}) = \gamma \left(-\frac{\vec{M}_0}{2} \cdot \vec{r} + B_{Off}(\vec{r}) \cdot \delta \right) \quad [6]$$

Therefore, the cumulative phase after the split refocused motion encoding gradient is insensitive to off-resonance:

$$\xi(\vec{r}) = \xi_1(\vec{r}) + \xi_2(\vec{r}) = -\gamma(\vec{M}_0 \cdot \vec{r}) \quad [7]$$

Therefore, the magnetization after the tagging preparation can be described as:

$$\vec{M} = \begin{bmatrix} -M_z^0 \sin(\xi_1(\vec{r}) + \xi_2(\vec{r})) \\ M_z^0 \cos(\xi_1(\vec{r}) + \xi_2(\vec{r})) \\ 0 \end{bmatrix} = \begin{bmatrix} -M_z^0 \sin(\gamma(\vec{M}_0 \cdot \vec{r})) \\ M_z^0 \cos(\gamma(\vec{M}_0 \cdot \vec{r})) \\ 0 \end{bmatrix} \quad [8]$$

Hence, the off-resonance effects during the interval of motion encoding are fully compensated.

Off-Resonance During Imaging

Signal phase accumulates during the interval of the readout gradient as a consequence of both the applied gradient and off-resonance. The off-resonance shift in the tagging pattern due to the phase accumulated during the readout gradient interval can be written as:

$$\Delta\varphi_{RO} = \frac{\Delta f}{BW} \quad [9]$$

where Δf is the frequency shift (Hz) between fat and water and BW is the readout gradient bandwidth (Hz/pixel).

During the first motion encoding experiment ($M_{SPAMM,1}$) the phase of the second 90 degree RF pulse is incremented ($\theta = 90^\circ$) and, subsequent to spoiling, the magnetization can be written in terms of the sinusoidal tagging pattern and the off-resonance shift during the readout gradient as,

$$M_{SPAMM,1} = M_z^0 \sin(\gamma(\vec{M}_0 \cdot \vec{r}) + \Delta\varphi_{RO}) \sin(\alpha) \quad [10]$$

where α is the RF imaging flip angle. During the second motion encoding experiment ($M_{SPAMM,2}$) the phase of the second RF is cycled to $\theta = -90^\circ$ and the magnetization after the second phase-cycling step can be written as:

$$M_{SPAMM,2} = M_z^0 \sin(-\gamma(\vec{M}_0 \cdot \vec{r}) + \Delta\varphi_{RO}) \sin(\alpha) \quad [11]$$

The CSPAMM tagging pattern is generated by the difference between the two phase-cycling loops, where the off-resonance term can be isolated from the spatially dependent tagging pattern term:

$$\begin{aligned} M_{ORI-CSPAMM} &= M_{SPAMM,2} - M_{SPAMM,1} \\ &= [M_z^0 \sin(-\gamma(\vec{M}_0 \cdot \vec{r}) + \Delta\varphi_{RO}) - M_z^0 \sin(\gamma(\vec{M}_0 \cdot \vec{r}) + \Delta\varphi_{RO})] \sin(\alpha) \end{aligned} \quad [12]$$

After applying the product-to-sum trigonometric identities for sine and cosine, Eq. [(12)] can be simplified to:

$$M_{ORI-CSPAMM} = -2M_z^0 \sin(\gamma(\vec{M}_0 \cdot \vec{r})) \cos(\Delta\varphi_{RO}) \sin(\alpha) \quad [13]$$

Thus, the phase of the tagging pattern is unaffected by off-resonance. However, the intensity of the tagged image will be diminished by the readout off-resonance term ($\cos\Delta\varphi_{RO}$).

MATERIALS AND METHODS

Healthy Subjects MRI Protocol

Healthy human subjects ($n = 13$) with no history of cardiovascular or respiratory disease were studied (3 female, mean age of 32.5 ± 11.2 years, weight 70.5 ± 12.7 kg, height 1.7 ± 0.1 m, heart rate 54.8 ± 9.2 beats/min). The local institutional review board approved this study and all subjects provided written informed consent.

ECG triggered images were acquired at end-expiration with subjects placed in the head-first supine position. All images were acquired with a Siemens Avanto 1.5 Tesla (T) scanner (Siemens Healthcare, Erlangen, Germany) and a six element body matrix coil in combination with a six-element spine matrix. Axial, coronal, and sagittal orientation scout images were used to plan the study. Balanced steady-state free precession cine images were acquired using a 6 mm slice thickness and a 66% gap between slices, in parallel left ventricular (LV) short-axis planes and used to select basal and apical slices for acquisition of tagged images. The most apical slice containing the presence of the blood pool throughout the entire cardiac cycle and the most basal slice in which the LV myocardium maintained a continuous annular shape during the entire cardiac cycle were used to prescribe the two slices for tagging and subsequent image processing.

The Siemens product cardiac gated spoiled gradient echo sequence was modified to support 1-1 binomially weighted SPAMM line tags and 1-1 binomially weighted CSPAMM and ORI-CSPAMM line tags (both with a total tagging flip angle of 180°). These sequences were used to acquire in vivo short-axis images at the base and apex of the LV with the following parameters: $360\text{--}300 \times 300\text{--}280$ mm field-of-view, 5–6 mm slice thickness, 192×144 acquisition matrix, 501 Hz/pixel receiver bandwidth, echo time/repetition time (TE/TR) = 3.5–3.7/4.7–6.5 ms, 7–8 views per segment, 10 mm tag spacing, and 14–16 cardiac phases. The breath hold duration (total scan time) for each sequence were 21 and 22 heart beats respectively (19.6 ± 4.1 s depending upon heart rate), for SPAMM and ORI-CSPAMM, respectively. The SPAMM data were acquired using two averages to maintain comparable SNR to CSPAMM and ORI-CSPAMM. The ORI-CSPAMM data was acquired without averaging, but required acquisition of two image sets with 180° RF phase cycling of the second tagging RF pulse. Additionally, a 15° imaging flip angle was used to acquire SPAMM images, while a non-linearly ramped flip angle (final 22°) was used to acquire CSPAMM

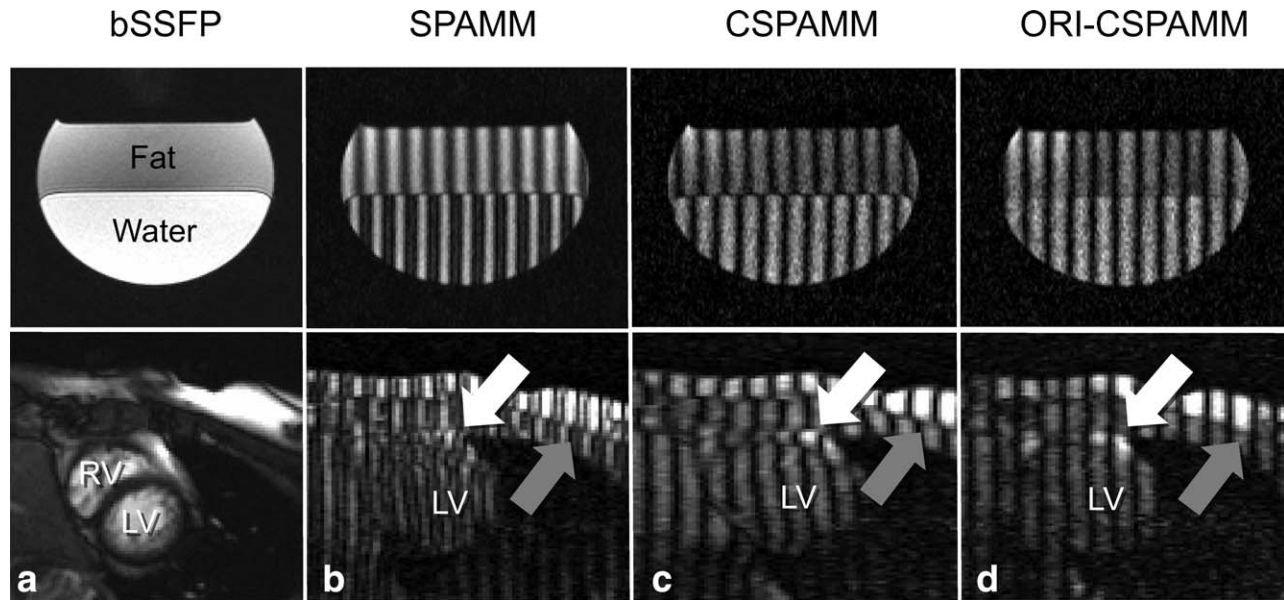


Figure 2. Images collected from a fat-water phantom (Row 1) and a healthy volunteer (Row 2) are presented. **a:** Demonstration of phantom set-up and in vivo anatomy. **b:** Chemical shift is apparent between water and fat (phantom) epicardial fat and myocardium (white arrow) and between chest wall fat and muscle (gray arrow) (in vivo) when using conventional 1-1 SPAMM tagging preparation. **c:** Chemical shift is apparent between water and fat (phantom) epicardial fat and myocardium (white arrow) and between chest wall fat and muscle (gray arrow) (in vivo) when using conventional 1-1 CSPAMM tagging preparation. **d:** In phantom and in vivo ORI-CSPAMM tag preparation, where chemical shift induced tagging pattern displacement is no longer visible due to the additional refocusing RF pulse.

and ORI-CSPAMM images (8). Cine tagged images were acquired using both horizontal and vertical tagging in separate breath holds.

Phantom MRI Protocol

A phantom was constructed using vegetable oil and water (Fig. 2, Row 1) to better demonstrate the effect of ORI-CSPAMM on tag alignment. The phantom was scanned using SPAMM, CSPAMM, and ORI-CSPAMM sequences with the following parameters: 199×199 mm field-of-view, 5 mm slice thickness, 192×192 acquisition matrix, 501 Hz/pixel receiver bandwidth, TE/TR=4.7/5.7ms, 8 views per segment, 10 mm tag spacing, and 20 cardiac phases. Averaging and imaging flip angles matched the healthy subject protocol.

Fourier Analysis of Stimulated echoes (FAST)

Manual contouring of the LV epicardium at an end-systolic frame and the endocardium in an early systolic frame was performed for both the apical and basal slices. The FAST (4) method uses the fact that rotation in image space corresponds to rotation in Fourier space. Subsequent to manual contouring, the FAST method performed least squares fitting of an ellipse to the respective LV boundary. The long and short axes of the ellipses were used to define a two-dimensional (2D) Butterworth mask that isolates the region of interest (LV) in all cardiac frames and suppressed the blood pool in the first three cardiac frames. Later in the cardiac cycle tags in the blood pool dissipate making the endocardial filter

unnecessary. The segmented image was then Fourier transformed after which the free induction decay was nulled with a circular mask and the Fourier image was cropped to the central 64 lines in k -space, leaving only the stimulated echo and anti-echo, which rotate in Fourier space. The final step of the FAST algorithm involved 2D cross-correlation in Fourier space with the subsequent cardiac frame to estimate the inter-frame rotation. Inter-frame rotations are calculated for all cardiac frames, from which values of LV twist were derived.

To determine rotation in the first cardiac frame the image is processed twice. First, the frame is processed identically to the method described above. Second, a copy of the first frame is made, segmented with the above-described Butterworth mask, and subsequently Fourier transformed. The copied first frame was then reflected about the axis perpendicular to the tagging lines, the FID was nulled, and the reflected image was cropped as described above. Finally, the reflected version of the first cardiac frame was 2D cross-correlated with the original segmented, nulled, and cropped first cardiac frame to estimate the first frame's rotation.

LV twist was calculated as the difference between the apical angle of rotation and basal angle of rotation for matching temporal frames with units of degrees (deg). Peak twist was identified as the maximum twist value for each subject. LV torsion was defined as LV twist divided by the distance between the apical and basal slices with units of deg/cm. Peak torsion was identified as the maximum torsion value for each subject. The circumferential-longitudinal shear angle (CL-shear angle) was defined as (9):

$$CL - Shear = \frac{\phi_{apex}\rho_{apex} - \phi_{base}\rho_{base}}{D}$$

where ϕ is rotation of the apex or base in degrees, ρ is the epicardial radius of the apex or base in mm, and D is the distance between the apex and base in mm. Peak CL-shear angle was identified as the maximum CL-shear angle for each subject. Twist rate was calculated as the temporal discrete derivative of twist with units of deg/s. Peak twist rate was identified as the maximum twist rate, while peak diastolic untwist rate was identified as the minimum twist rate. Normalized peak untwist rate was calculated as the minimum twist rate divided by the maximum twist angle with units of s^{-1} .

Data Processing

The FAST+ORI-CSPAMM and FAST+SPAMM estimates of rotation were used for statistical analysis of peak twist, torsion, twist rate, and untwist rate, mean peak values and timings for the apical and basal slices, and time of peak twist. The duration of untwisting was determined from twist data interpolated with a cubic smoothing spline to 1% increments of the cardiac cycle. This smoothing reduced noise and allowed for better detection of the end of untwisting, the maximum of the second derivative of the twist after peak systolic twist. The end of rapid untwisting was used to estimate the ratio of rapid untwisting to peak twist. Atrial systole completes the process of untwisting in healthy hearts. The ratio of rapid untwisting to peak twist provides insight into the contribution of atrial systole to the completion of the untwisting process. Additionally, tag motion becomes undetectable due to tag fading in SPAMM images; as a result, all SPAMM data were truncated to the first 500 ms of the cardiac cycle. Tag fading occurs as a result of T1 relaxation of the tagging pattern and from the component of the image intensity derived from relaxation after the application of the tagging pattern (7). The CSPAMM pulse sequence was specifically designed to mitigate the effect of tag fading by separating the relaxed component of the magnetization from the tagging pattern by phase cycling the second tagging RF pulse and subtracting the phase cycled images. ORI-CSPAMM improves tag contrast as a result of the CSPAMM tagging pattern and removes the chemical shift artifact in the tagging pattern compared with traditional SPAMM tagging.

Figure 3 depicts the systolic and diastolic measures of twist calculated with FAST+ORI-CSPAMM and FAST+SPAMM. Peak systolic twist, systolic twist rates, and early diastolic untwisting are clearly visible for both FAST+ORI-CSPAMM and FAST+SPAMM results (Fig. 3). FAST+ORI-CSPAMM results, however, also clearly show the end of diastolic untwisting and continue into mid-diastasis. Figure 3 shows incomplete diastolic untwisting in the case of SPAMM because the tags have faded too much for quantitative analysis.

Statistical Analysis

Comparisons between FAST+ORI-CSPAMM and FAST+SPAMM were only performed for the first 500

ms of the cardiac cycle due to tag fading in the SPAMM images. Linear regression analysis with a forced zero intercept and calculation of Pearson’s correlation coefficient (r) were performed to compare FAST+ORI-CSPAMM with FAST+SPAMM for healthy subject twist, torsion, and twist rate. The Wilcoxon signed-rank test for paired non-parametric samples, as well as, paired t-test with Bonferroni post hoc correction for multiple comparisons were used to compare peak systolic twist, torsion, and CL-shear angle, as well as, peak twisting and untwisting rates. A $P < 0.01$ was considered statistically significant after the post hoc correction. Additionally, a paired t-test was used to compare FAST+ORI-CSPAMM and FAST+SPAMM twist, torsion, and twist rate values for first 500 ms of the cardiac cycle after data de-correlation using a decimation interval equivalent to the first zero crossing of the autocorrelation (autocorrelation length of 3.4 ± 0.4 cardiac phases) of the respective curves. A Bland-Altman analysis was performed to compare peak twist and torsion values measured using FAST+ORI-CSPAMM and FAST+SPAMM. A Kolmogorov-Smirnov test for normality was performed on the peak twist data, which demonstrated the non-Gaussian nature of the data. Due to the small sample size and the non-Gaussian data, the 95% confidence intervals were determined by bootstrapping the median of the biases (FAST+ORI-CSPAMM minus FAST+SPAMM), by sampling with replacement 10,000 times. The median of the bootstrapped data instead of the mean was selected for a better representation of the “typical” peak twist value. The Bland-Altman bias is reported as the median of the biases. Peak data values were reported as mean \pm one standard deviation with the inter-subject range of values in parenthesis when applicable.

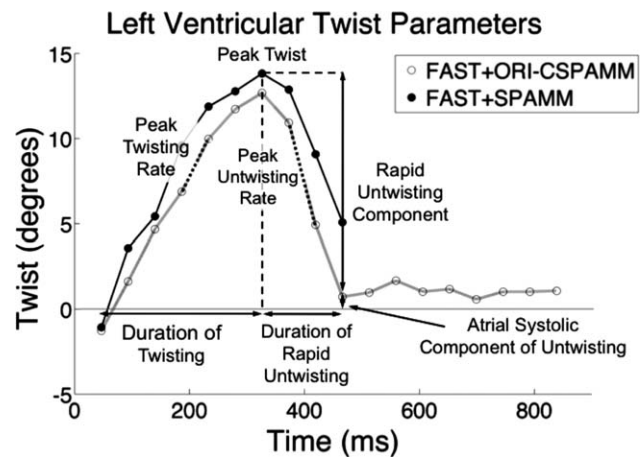


Figure 3. LV twist parameters that are enabled by FAST+SPAMM and FAST+ORI-CSPAMM include peak twist, peak twisting rate, peak untwisting rate, duration of twisting, duration of rapid untwisting, and the ratio of rapid untwisting to peak twist, which gives insight into the atrial systolic component of untwisting. Note that the FAST+SPAMM curve was truncated to the first 500 ms of the cardiac cycle due to tag fading.

RESULTS

There was no significant difference for measures of peak twist derived from FAST+ORI-CSPAMM and FAST+SPAMM in normal subjects ($12.9 \pm 2.7^\circ$ versus $11.9 \pm 4.0^\circ$, $P=0.4$). Mean peak torsion derived from FAST+ORI-CSPAMM and FAST+SPAMM were not significantly different ($3.3 \pm 0.9^\circ/\text{cm}$ versus $2.9 \pm 1.0^\circ/\text{cm}$, $P=0.3$). Mean peak CL-shear angle derived from FAST+ORI-CSPAMM and FAST+SPAMM were not significantly different ($9.1 \pm 3.0^\circ$ versus $8.2 \pm 3.4^\circ$, $P=0.3$). Mean peak twist rates derived from FAST+ORI-CSPAMM and FAST+SPAMM were $79.6 \pm 20.2^\circ/\text{s}$ and $68.2 \pm 23.4^\circ/\text{s}$ ($P=0.1$). Mean peak untwist rate from FAST+ORI-CSPAMM and FAST+SPAMM was $-117.5 \pm 31.4^\circ/\text{s}$ versus $-106.6 \pm 32.4^\circ/\text{s}$ ($P=0.3$). Mean peak normalized untwist rate derived from FAST+ORI-CSPAMM and FAST+SPAMM was $-9.3 \pm 2.0/\text{s}$ versus $-9.9 \pm 4.4/\text{s}$ ($P=0.7$). The Wilcoxon signed rank test did not reveal any significant differences for the peak values stated above (all $P > 0.01$). The mean time to peak twist was 281 ± 18 ms and 293 ± 25 ms for FAST+ORI-CSPAMM and FAST+SPAMM, respectively ($P=0.04$). The mean duration of untwisting was 148 ± 21 ms measured with FAST+ORI-CSPAMM. The mean ratio of rapid untwisting to peak twist ratio was 0.9 ± 0.3 measured with FAST+ORI-CSPAMM. Both the duration of untwisting and the ratio of rapid untwisting to peak twist could not be accurately measured with FAST+SPAMM due to tag fading.

Bland-Altman analysis for peak FAST+ORI-CSPAMM twist and torsion data was compared with the FAST+SPAMM data (Fig. 4). There was good agreement between ORI-CSPAMM and SPAMM for calculating LV twist (bias of -0.1° and 95% confidence intervals of $[-1.0^\circ, 3.2^\circ]$) and torsion (bias of $-0.01^\circ/\text{cm}$ and 95% confidence intervals of $[-0.3^\circ/\text{cm}, 0.8^\circ/\text{cm}]$), respectively. Bland-Altman analysis for peak CL-shear angle had a bias of -0.3° and a 95% confidence interval of $(-1.1^\circ, 2.3^\circ)$. Bland-Altman analysis for peak systolic twist rate and diastolic untwisting rate provided a bias of $18.8^\circ/\text{s}$ and $-24.51^\circ/\text{s}$ a 95% confidence intervals of $(-6.1^\circ/\text{s}, 24.4^\circ/\text{s})$ and $(-36.1^\circ/\text{s}, 9.9^\circ/\text{s})$, respectively.

Linear regression analysis for the first 500 ms of the cardiac cycle using the FAST+ORI-CSPAMM and FAST+SPAMM data yielded a Pearson's correlation coefficients of $r=0.82$ and the equation $\text{ORI-CSPAMM} = 0.95 * \text{SPAMM}$ for the twist results and $r=0.82$ and the equation $\text{ORI-CSPAMM} = 0.95 * \text{SPAMM}$ for the torsion results, respectively. Linear regression analysis of twist rate, which includes twisting and untwisting, provided $r=0.88$ and the equation $\text{ORI-CSPAMM} = 0.97 * \text{SPAMM}$. The paired t-test of the decimated data for the twist, torsion, and twist rate curves did not reveal any significant differences between FAST+ORI-CSPAMM and FAST+SPAMM, $P > 0.8$.

The average user interaction time for the FAST method was 2.6 ± 0.3 min. This time includes study selection and contouring of the epicardium and endocardium for the basal and apical slices for both horizontal and vertical tags. The average postprocessing

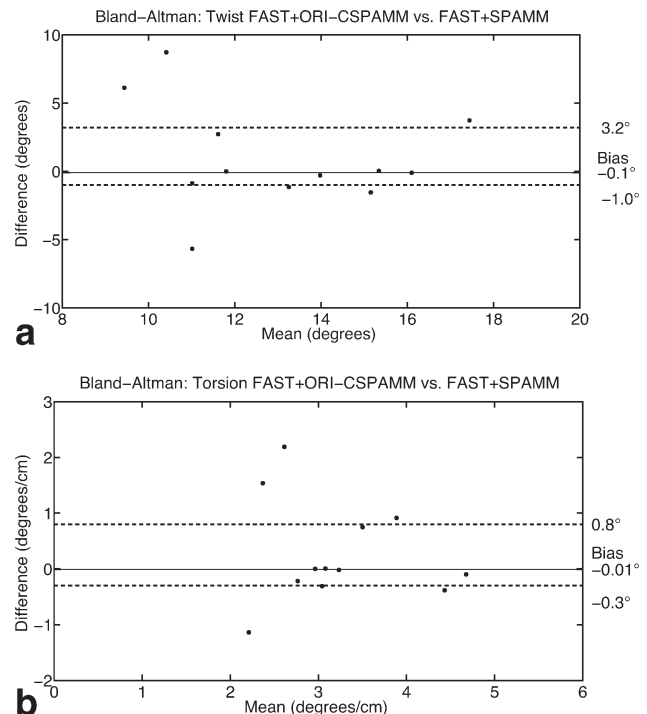


Figure 4. Bland-Altman analysis of LV twist estimates (a) from FAST+ORI-CSPAMM compared with FAST+SPAMM for the peak values indicates good agreement. The comparison of LV twist measures has a bias of -0.1° and a variance of $(-1.0^\circ, 3.2^\circ)$. Bland-Altman analysis of LV torsion estimates (b) from FAST+ORI-CSPAMM compared with FAST+SPAMM for the peak values indicates good agreement. The comparison of LV torsion measures has a bias of -0.01° and a variance of $(-0.3^\circ, 0.8^\circ)$.

computational time of four series of tagged images was approximately 21 min performed on a MacBook Pro with a 2.4 GHz Intel Core 2 Duo processor.

Qualitative Image Assessment

The ORI-CSPAMM sequence completely removes the chemical shift displacement effect from the phase of the tagging pattern (Fig. 2). In SPAMM (Fig. 2B), the chemical shift in the tagging pattern arises as a function of the duration of the motion encoding gradient and the readout gradient. The shift in the periodicity of the SPAMM tagging pattern is ~ 4.4 pixels in phantom and ~ 2.4 pixels in vivo between oil (i.e., fat) and water. For CSPAMM (Fig. 2C), the shift in periodicity of the tagging pattern is ~ 8.4 pixels in phantom and ~ 4.4 pixels in vivo between oil and water. Figure 2D, clearly illustrates that the chemical shift in the tagging pattern has been removed as predicted by the ORI theory. This is apparent in both in the chest wall between subcutaneous fat and muscle and in the heart at the myocardial-epicardial fat boundary.

DISCUSSION

FAST+ORI-CSPAMM provides an automated method for the quantitative assessment of LV systolic and diastolic twist, torsion, twisting rate, untwisting rate,

normalized untwisting rate, and time to peak twist subsequent that is insensitive to off-resonance. Unlike the fat suppression CSPAMM sequence proposed by Fahmy et al (6), ORI-CSPAMM removes the effects of off-resonance to the tagging pattern, however the tag intensity of off-resonant tissues has a residual effect. In Fourier space, where FAST image processing occurs, ORI-CSPAMM provides more easily detectable peaks (stimulated echoes and stimulated anti-echoes) later into the cardiac cycle than FAST+SPAMM, which allows reliable access to complete early diastolic untwisting.

In the healthy heart, epicardial fat is a primary source of off-resonant tissue. It should, however, lie outside the region of interest used for FAST twist calculations. Thus, no significant differences between FAST twist measurements made with the ORI-CSPAMM and SPAMM were detected in this work. Nevertheless, there is a trend to higher reported systolic twist related parameters when using ORI-CSPAMM, which is consistent with the expectation from theory. For example, when tag analysis inadvertently includes tags that reside in the epicardial fat, then rotation estimates will be over- or underestimated when using FAST, unless ORI-CSPAMM is being used. The over- or underestimation in rotation is due to the discontinuity in the tagging pattern between the myocardium and the epicardial fat, which contributes an apparent rotation. Hence, the shifted fat tags contribute an additional rotation, which is easily detected with FAST or another tag tracking technique. Similarly, in patient populations with fatty infiltration of the LV (10,11), FAST+ORI-CSPAMM maybe particularly useful in providing accurate twist measurements.

Bland-Altman results show a good agreement between FAST+ORI-CSPAMM and FAST+SPAMM, and there were no statistical differences between the two methods for the first 500 ms of the cardiac cycle. These results indicate that for systole and early diastole FAST+ORI-CSPAMM and FAST+SPAMM yield nearly equivalent results as expected. The values of peak twist, peak torsion, peak twisting rate, and peak untwisting rate matched well with literature values of $12.7 \pm 1.7^\circ$ (12), $1.9 \pm 0.3^\circ/\text{cm}$ (12), $85.9 \pm 28.6^\circ/\text{s}$ (13), and $-114.6 \pm 40.1^\circ/\text{s}$ (13), respectively. However, the value of peak CL-shear angle differed slightly from previously reported values $7.7 \pm 1.2^\circ$ (14). The difference between the value reported in this study and that of the literature may be due to the selection of a more basal apical slice in this study. This selection of apical slice location leads to a larger apical epicardial radius and a smaller distance between the slice, which both contribute to the larger CL-shear angle value reported in this study. Shear angle has been reported to be a more robust measure of rotational mechanics than twist or torsion, however, this may not be the case as demonstrated by the difference reported in this study compared with a typical literature value.

There are two important limitations to this study. First, clinical patients were not included in this study. To better understand how fatty infiltration affects twist measurements made from tagged MR images, a

clinical study should be performed. Second, phase-cycling used to generate CSPAMM images leads to longer breathhold durations when compared with SPAMM, making ORI-CSPAMM acquisitions challenging for patients with limited breathhold capabilities. These longer breathholds may also contribute to changes in twist/torsion between acquisitions, due to changes in loading conditions of the heart. Improvements in acquisition efficiency may be overcome with higher parallel imaging acceleration rates or the incorporation of prospective compressed sensing.

In conclusion, FAST+ORI-CSPAMM quickly and quantitatively calculates systolic and diastolic LV twist, torsion, CL-shear angle, twisting rates, time to peak twist, duration of untwisting, and the ratio of rapid untwisting to peak twist. ORI-CSPAMM corrects off-resonance accrued during tagging preparation and readout and visibly removes chemical shift from the tagging pattern, which confers greater robustness to the derived quantitative measures.

ACKNOWLEDGMENTS

D.B.E. was funded by NIH/NHLIB and M.L.R. was funded by the AHA.

REFERENCES

1. Axel L, Dougherty L. MR imaging of motion with spatial modulation of magnetization. *Radiology* 1989;171:841-845.
2. Aletras AH, Ding S, Balaban RS, Wen H. DENSE: displacement encoding with stimulated echoes in cardiac functional MRI. *J Magn Reson* 1999;137:247-252.
3. Osman N, Kerwin W, McVeigh E, Prince J. Cardiac motion tracking using CINE harmonic phase (HARP) magnetic resonance imaging. *Magn Reson Med* 1999;42:1048-1060.
4. Reyhan M, Natsuaki Y, Ennis DB. Fourier analysis of STimulated echoes (FAST) for the quantitative analysis of left ventricular twist. *J Magn Reson Imaging* 2012;35:587-593.
5. Middione MJ, Ennis DB. Chemical shift-induced phase errors in phase-contrast MRI. *Magn Reson Med* 2013;69:391-401.
6. Fahmy AS, Basha TA, Osman NF. Inherent fat cancellation in complementary spatial modulation of magnetization. *Magn Reson Med* 2009;61:234-238.
7. Fischer SE, McKinnon GC, Maier SE, Boesiger P. Improved myocardial tagging contrast. *Magn Reson Med* 1993;30:191-200.
8. Stuber M, Spiegel MA, Fischer SE, et al. Single breath-hold slice-following CSPAMM myocardial tagging. *MAGMA* 1999;9:85-91.
9. Russel IK, Tecelao SR, Kuijter JP, Heethaar RM, Marcus JT. Comparison of 2D and 3D calculation of left ventricular torsion as circumferential-longitudinal shear angle using cardiovascular magnetic resonance tagging. *J Cardiovasc Magn Reson* 2009;11:8.
10. Kies P, Bootsma M, Bax J, Schalij MJ, van der Wall EE. Arrhythmogenic right ventricular dysplasia/cardiomyopathy: screening, diagnosis, and treatment. *Heart Rhythm* 2006;3:225-234.
11. Nishimura T, Yanagisawa A, Sakata H, et al. Thallium-201 single photon emission computed tomography (SPECT) in patients with duchenne's progressive muscular dystrophy: a histopathologic correlation study. *Jpn Circ J* 2001;65:99-105.
12. Henson RE, Song SK, Pastorek JS, Ackerman JJ, Lorenz CH. Left ventricular torsion is equal in mice and humans. *Am J Physiol Heart Circ Physiol* 2000;278:H1117-H1123.
13. Notomi Y, Martin-Miklovic MG, Oryszak SJ, et al. Enhanced ventricular untwisting during exercise: a mechanistic manifestation of elastic recoil described by Doppler tissue imaging. *Circulation* 2006;113:2524-2533.
14. Russel IK, Brouwer WP, Germans T, et al. Increased left ventricular torsion in hypertrophic cardiomyopathy mutation carriers with normal wall thickness. *J Cardiovasc Magn Reson*; 13:3.